HHS Public Access

Author manuscript

*Neuroimage*. Author manuscript; available in PMC 2016 July 01.

Published in final edited form as:

*Neuroimage*. 2015 July 1; 114: 320–327. doi:10.1016/j.neuroimage.2015.04.001.

# Context-specific differences in fronto-parieto-occipital effective connectivity during short-term memory maintenance

**Bornali Kundu**[1], **Jui-Yang Chang**[2], **Bradley R. Postle**[1,3], and **Barry D. Van Veen**[2]

[1]Neuroscience Training Program and Medical Scientist Training Program, University of Wisconsin—Madison, 7225 Medical Sciences Center, 1300 University Avenue, Madison, WI 57306, USA

[2]Department of Electrical and Computer Engineering, University of Wisconsin-Madison, 3611 Engineering Hall, 1415 Engineering Drive, Madison, WI 53706

[3]Department of Psychology, University of Wisconsin-Madison, 1202 West Johnson Street, Madison, WI 53706, USA

## Abstract

Although visual short-term memory (VSTM) performance has been hypothesized to rely on two distinct mechanisms, capacity and filtering, the two have not been dissociated using network-level causality measures. Here, we hypothesized that behavioral tasks challenging capacity or distraction filtering would both engage a common network of areas, namely dorsolateral prefrontal cortex (dlPFC), superior parietal lobule (SPL), and occipital cortex, but would do so according to dissociable patterns of effective connectivity. We tested this by estimating directed connectivity between areas using conditional Granger causality (cGC). Consistent with our prediction, the results indicated that increasing mnemonic load (capacity) increased the top-down drive from dlPFC to SPL, and cGC in the alpha (8−14 Hz) frequency range was a predominant component of this effect. The presence of distraction during encoding (filtering), in contrast, was associated with increased top-down drive from dlPFC to occipital cortices directly and from SPL to occipital cortices directly, in both cases in the beta (15−25Hz) range. Thus, although a common anatomical network may serve VSTM in different contexts, it does so via specific functions that are carried out within distinct, dynamically configured frequency channels.



**Corresponding author:** Bornali Kundu (Health Emotions Research Institute, 6001 Research Park Blvd, Rm 1056, Madison, WI 537019, (608)-265-8961, bkundu@wisc.edu).



**COMPETING FINANCIAL INTERESTS**

The authors declare no competing financial interests.

**AUTHOR CONTRIBUTIONS**

B.K. and B.R.P. designed the study; B.K and B.D.V developed the analysis plan; B.K. performed the experiments; B.K. and J.Y. analyzed data; and all authors contributed to the writing of the manuscript.

**Keywords**

Granger causality; electroencephalogram; short-term memory; attention; effective connectivity; multivariate autoregressive models

## INTRODUCTION

A growing body of evidence suggests that visual short-term memory (VSTM), and the related construct of working memory, may share common neural bases with selective attention (e.g. Nobre and Stokes, 2011; D'Esposito and Postle, 2015). In the domain of spatial cognition, for example, both engage a highly overlapping network of frontoparietal regions (e.g., Ikkai and Curtis, 2011), from which information can be "read out", depending on context, to accomplish oculomotor, attentional, or mnemonic goals (Jerde et al., 2012). Additionally, training on a visual working memory task has comparable effects on event-related potential (ERP) components associated with VSTM (the contralateral delay activity; CDA) and with visual selective attention (the contralateral search activity (CSA) (Kundu et al., 2013), suggesting that there is a relationship between the underlying mechanisms supporting VSTM and visual selective attention. The CDA is an ERP component derived during a VSTM task, for which the amplitude scales monotonically with the number of items being held in VSTM, and plateaus at an individual's VSTM capacity (Vogel and Machizawa, 2004). The CSA is an ERP component derived during visual search for which the amplitude correlates with individual differences in VSTM capacity (Emrich et al., 2010).

One influential model of attentional control, operationalized through the Attentional Network Task, is organized into three dissociable components: alerting, orienting, and executive control (Fan et al., 2002). Machizawa and Driver (2011) related this framework to working memory by applying a principal components analysis to a behavioral dataset, and found that not only did putative measures of alerting, orienting, and executive control load independently onto the first three principle components, but so too did measures relating to three constructs from VSTM: capacity, precision, and filtering, respectively. In this paper we focus on the constructs of capacity and filtering. The former, in particular, has been of interest due to its ability to predict individual variation in cognitive measures such as search efficiency (Emrich et al., 2010) and filtering efficiency (Vogel et al., 2005), as well as higher-order measures such as educational achievement (Cowan et al., 2005; c.f. Cusack et al., 2009). Although capacity and filtering have both been related to the CDA (Vogel and Machizawa, 2004; Vogel et al., 2005), the two have not, to our knowledge, been dissociated at the network level. The goal of this study, therefore, was to interrogate the dorsal frontoparietal network with a method capable of detecting context-dependent differences in its EEG dynamics.

Specifically, we tested whether there is evidence of systematic differences in effective connectivity within a network comprising dorsolateral prefrontal cortex (dlPFC), superior parietal cortex (SPL), and extrastriate cortex during the delay-period of a VSTM task that emphasized either capacity or filtering. The rationale for choosing these areas lies in the findings from Kundu et al. (2013) which showed that working-memory training increases

transcranial magnetic stimulation (TMS)–based measures of effective connectivity between dlPFC and SPL, as well as between SPL and extrastriate visual areas. It also showed that connectivity between dlPFC and SPL increase with VSTM load. Importantly, single pulse TMS provides a measure of effective connectivity such that we know exactly where and when stimulation occurred and thus we can measure its downstream effects in time through a data-driven manner (Casali et al., 2010). However, this method is limited in that it can only address the relative differences in connection strengths between the area stimulated and other distal areas. It cannot probe a predetermined connection between any two regions. Thus, the present study builds on the network model implicated by Kundu et al., (2013), but tests the hypothesis that different task contexts will be associated with systematic variation in the strength and direction of connectivity within the network.

This was accomplished using high-density (EEG) data and a recently developed method (Cheung et al., 2010) to estimate the conditional Granger causality (cGC) metric (Bressler and Seth, 2011) between dlPFC, SPL, and occipital cortex. Thus this method measures effective connectivity in its simplest sense, which is the change in electrical activity at one location as a weighted sum of changes elsewhere (Friston, 1994; and as explicated by us previously in Dentico et al. (2014) and Piatoni et al. (2013)). We do note, however, that the term ‘effective connectivity’ has also been used to refer more specifically to causal interactions measured in neurobiologically based models, such a dynamic causal modeling (see Friston, 2011 for a review.) Such measures of effective connectivity can address the precise chronometry between networks that act as candidate sources of top-down control (Miller and D’Esposito, 2005). We hypothesized that increases in memory load and increases in filtering demands would produce differences in the strength and/or direction of effective connectivity between dlPFC and SPL, as well as between these areas and extrastriate occipital cortex, depending on context.

## METHODS

### Participants

Data reported in the present study were taken from the pre-training session of a working memory training study (Kundu et al., 2013). 30 participants (16 female, mean age = 20.9 years, *SD* = 2.75 years) were recruited for the study from the University of Wisconsin-Madison community. The inclusion criteria selected healthy participants between the ages of 18–35 years, with normal or corrected-to-normal visual acuity and normal color vision, and who were not currently taking medication for psychiatric conditions. All procedures were approved by the University of Wisconsin-Madison Institutional Review Board.

### Overview of tasks

Two tasks were used to test short-term memory (STM). The location VSTM and Target-epoch distraction (TD) tasks were selected because they operationalize two theoretical factors -- capacity and filtering, -- hypothesized to account for individual differences in STM and selective attention (Machizawa and Driver, 2011). Each subject performed the location VSTM task and then the TD task.

**Location VSTM Task—**The trial began with a cue indicating the visual hemifield that was relevant for that trial. Then, either two (Load 2) or four (Load 4) black squares ("target stimuli") were presented serially in the cued hemifield, along with a comparable, simultaneous sequence in the uncued hemifield ("foil stimuli"). Load condition varied randomly (without replacement) on a trial-by-trial basis, as did the location of each target and foil, which was determined by using a random number generator to generate coordinates within a predetermined area of the visual field. Then there was a delay period of 3750 ms after which a probe that either did or did not match ($P = 0.5$) the location of one of the stimuli appeared (Fig. 1A). Subjects were instructed to maintain central fixation throughout the delay. The subjects indicated whether the probe matched the location of any one of the memory targets presented in the cued hemifield via left/right button press at the end of the trial. Subjects used both of their hands, right thumb for the right button and left thumb for the left button. Left and right button assignments indicated match and non-match responses respectively. These button assignments were the same across subjects (i.e. button assignment was not counterbalanced). Note, counterbalancing was not required because the analyses were restricted to the delay period, when no responses were being made, and when subjects could not predict what the response would be. The probe always appeared in the cued hemifield. Feedback was provided on a trial-by-trial basis, with the word "Incorrect" appearing on the screen for 500 ms following an incorrect response. The intertrial interval (ITI) was 550 ms. The task block consisted of 480 trials presented in sub-blocks of 60 trials. Two transcranial magnetic stimulation (TMS) pulses were delivered during the delay period of 50% of the trials, selected at random. The data from the TMS-present trials will not be discussed in this report. The participants received verbal instructions and completed a block of trials prior to testing. The practice blocks were repeated until a criterion of 75% accuracy was reached. No more than three practice blocks were required for any subject. Memory targets were presented within a 4.3° x 8.6° region in hemifield, centered ∼3.3° horizontally from fixation. Memory targets consisted of black squares subtending ∼1° of visual angle at a viewing distance of 70 cm and were presented on a gray background. The probe consisted of a black square (∼1° of visual angle). The probe for non-match trials was presented at a randomly chosen location within the cued hemifield and at a minimum of 2.5° (center-to-center distance) away from the nearest memory target location.

**Target-epoch distraction (TD) task—**This task was a variant of the location VSTM task (Fig. 1B) and two of three trial types, *Load 2* and *Load 4*, were similar to those from the location VSTM task. The third trial type, *Load 2d*, was a trial with two relevant black squares and two blue distractor squares serially presented in a random order within the cued hemifield. Subjects were instructed to retain the locations of the black squares and ignore the locations of the blue squares. There were 120 trials per condition organized in 6 sub-blocks. The delay period of 2000 ms had no distraction. The same button assignments were used for this task as the VSTM task. Left and right button assignments indicated match and non-match responses respectively. The button assignments for particular responses were not counterbalanced across subjects in this task. Analyses from this task are limited to *Load 2* versus *Load 2d* for consistency with the comparison between *Load 2* versus *Load 4 in* the location VSTM task.

**EEG recording—**EEG was recorded for the location VSTM task and the TD task with a 60-channel TMS-compatible amplifier (Nexstim; Helenski, Finland). Electrode impedance was <5kΩ. The reference and ground electrodes were placed on the forehead. Eye movements were recorded with two additional electrodes placed near the eyes. The EEG signal was filtered (0.1–500 Hz) and sampled at 1450 Hz with 16-bit resolution.

**Data pre-processing—**Data were processed offline using the EEGLab toolbox (Delorme and Makeig, 2004) as well as the Signal Processing ToolBox in MATLAB (Version 2012a). The data were downsampled to 103 Hz, average-referenced, and demeaned. Independent components analysis (ICA) was performed on usable channels to identify and remove components reflecting residual muscle activity, eye movements, blink-related activity, and residual TMS-related artifacts. High-pass filtering was applied at 2 Hz (Chebyshev Type II high pass filter, stopband frequency 1.5 Hz, passband frequency 3 Hz, stopband attenuation 30 dB, passband ripple 1 dB). Subject data that was found to have >70% of trials contaminated by noise, muscle artifact, or eye movement artifact during the task were excluded from the analyses.

**Network Regions-of-interest (ROIs)—**We hypothesized that differences in casual connectivity underlying capacity versus filtering would be seen in a network comprising occipital, posterior parietal, and prefrontal areas. Using the TMS-present trials from the location VSTM task, Kundu et al. (2013) showed that load-specific changes as well as training-related changes in TMS-based measures of effective connectivity were seen primarily between Brodmann Area (BA) 7 which is the SPL and BA 9 which is the dlPFC (see Table 2 of Kundu et al., 2013). Thus the TMS experiment used a causal method to define the network of areas that were 1) engaged by the task, and 2) whose connectivity was strengthened by training. If indeed the three hypothesized factors underlying attentional control also underlie VSTM performance then this network should be differently engaged by VSTM tasks that put differential demands on these putative factors. Thus, the present study included regions in the network implicated in Kundu et al. (2013) and included bilateral BAs 9, 7, and 18 (Fig. 2 A and B).

**MVAR model—**We employed a state-space MVAR model to derive measures of cortical casual connectivity from scalp data. The state-space approach has been shown to be more robust than conventional two-stage connectivity estimation methods at the low signal-to-noise ratios (SNRs) typical of EEG data (Cheung et al., 2010). Note that the model-derived cGC metric between two brain regions could, in principle, capture the influence of both cortico-cortical and cortico-thalamic pathways. We did not attempt to dissociate these effects. The cortical patches used to represent individual ROIs in the model were derived using the following steps: 1) Subject-specific whole-brain T1-weighted anatomical MRIs were acquired with a GE MR750 3T MRI scanner prior to the experiment (176 axial slices with a resolution of 1 mm); 2) Individual cortical meshes (5124 vertices) were created from the MRIs using the Statistical Parametric Mapping software package (SPM8, freely available at: http://www.fil.ion.ucl.ac.uk/spm/); 3) The meshes were co-registered with the individual's EEG sensor positions collected using a frameless stereotaxy system (part of the Navigated Brain Stimulation system used to deliver TMS); 4) The Boundary Element Model

(BEM) was used to model the physics of measurement of cortical signals at the electrode locations; 5) Individual cortical surfaces were attributed to different BAs using an automatic anatomical classification method that maps the individual cortical surface to the region of interest (ROI) masks provided by the WFUPickAtlas tool (freely available at: http://ansir.wfubmc.edu); 6) Following Cheung et al. (2010), the leadfield matrices of the dipoles in each ROI were concatenated and the left singular vectors, corresponding to the largest singular values, used as spatial bases representing the dominant activity from the ROI.

Conventional approaches to source localization first attempt to solve the inverse problem and estimate cortical signals from the scalp data. Next they attempt to fit an MVAR model to the estimated cortical signals. Such two-stage approaches require relatively high SNR to obtain accurate estimates of cortical connectivity. The state-space approach employed here directly estimates the model parameters in one step using an expectation-maximization (EM) algorithm that jointly solves the equations describing both the cortical MVAR model and the measurement physics. The following equations describe the method as applied to the data of the present study, see Cheung et al., (2010) for formal mathematical definitions of the model's general form. The state-space representation of the data is as follows.

$$x_{\pi,j}=\Lambda z_{\pi-1,j}+w_{\pi,j} \quad (1)$$

$$y_{\pi,j}=\mathrm{C}\Lambda x_{\pi,j}+v_{\pi,j} \quad (2)$$

Here $x_{\pi,\mathrm{j}}$ is the state variable representing the cortical signals from the six ROIs at time point *n* and epoch *j*. **A** is the 6 × 6*P* state-transition matrix and describes the influence of the past *n*-1 time points of *x*, contained in $Z_{n\text{-}1,j}$, on $x_{\pi,\mathrm{j}}$. *P* is the model order and is the number of past time samples considered. $w_{\pi,\mathrm{j}}$ is a 6 × 1 vector of error residuals predicting the present cortical signal based on its past, and is modeled as a series of identically distributed Gaussian vectors with zero mean and covariance matrix **Q** ($\sim$ N(0,**Q**)). $y_{\pi,\mathrm{j}}$ is the EEG data observed at the scalp for time *n* and epoch *j* over *L* number of channels based on the number of significant ICA components retained. **C** is an *L x* 6*K* matrix of the *K* left singular values from the singular value decomposition of the leadfields. $\Lambda$ is a 6*K x* 6 matrix that represents the unknown spatial distribution of activity within the ROIs. The unknown entries in $\Lambda$ are estimated as part of the EM algorithm (Cheung, et al. 2010). Finally, $v_{\pi,\mathrm{j}}$ is the observed noise and is assumed to be a series of independent, identically distributed Gaussian random vectors with mean 0 and unknown covariance matrix **R** ($\sim$ N(0,**R**)). Thus, Equation 1 is a "hidden" state equation describing the MVAR model between cortical regions. Equation 2 describes how the cortical signals are projected to the scalp based on the known variables of the leadfields and observed noise, as well as the unknown variables of the cortical signals, as well as their spatial distribution within an ROI.

Instead of solving the observation equation first and then fitting the model, this method uses the EM algorithm to do these steps simultaneously. We used a model order *P*=16 because it yielded stable measures of connectivity in the data of 3 subjects. A relatively small number of singular vectors has been shown to capture the activity in relatively large cortical regions (Limpiti et al., 2006), so in the present study *K*=3. This choice has been effective in other

studies using similar sized ROIs (Malekpour et al., 2012; Piantoni et al., 2013). Thus the known parameters are $y_{\pi,j}$ and **C**. The unknown parameters are **A**, $x_{\pi,j}$, Λ, **Q, R**. The EM algorithm is guaranteed to converge to a local maximum of the likelihood. We ran the algorithm multiple times using different initial conditions and selected the run with the maximum value of likelihood as our estimate. We initialized the model with 19 different sets of initial conditions.

**cGC**. cGC, described by Geweke (1984), is a measure casual connectivity, or the degree to which one brain area can causally influence another (Friston, 1994). For ROI time series $a_\pi$, $b_\pi$ and $c_\pi$ along with each series' past values ($a_{\pi-}$, $b_{\pi-}$ and $c_{\pi-}$) the cGC from *a to b* conditioned on *c* is as follows,

$$F_{a\to b\ c}=log\frac{|\Sigma_1|}{|\Sigma_2|} \quad (3)$$

where $\Sigma_1$ is the error covariance when predicting $b_\pi$ from its own past $b_{\pi-}$, and the past of $c_\pi$. $\Sigma_2$ is the error covariance of predicting $b_\pi$ from $a_{\pi-}$, $b_{\pi-}$, *and* $c_{\pi-}$. $F_{a\to b\ c}$ is guaranteed to be positive through use of the partitioned matrix method (Chen et al., 2006). We considered 6 time series from the 6 ROIs within the model. cGC was calculated by collapsing over the left and right hemispheres such that the joint cGC between bilateral pairs of hemispheres was considered (Fig. 2C).

Calculation of cGC in the frequency domain was done according to Chen et al., (2006). (Equations 22 onward in the Methods section of Chen et al., (2006) indicate a formulation of how cGC is computed in the frequency domain.) The method allows calculation of the portion of the total power of signal $b_\pi$ at frequency ω that is contributed by $a_\pi$ given $c_\pi$. In the context of the final model, shown in Figure 2C, signals $a_\pi$, $b_\pi$, and $c_\pi$ are vectors containing signals from both hemispheres. For example, cGC tells us how well the past of the left and right hemisphere signals from BA 9 predict the present of the left and right hemisphere signals in BA 7 given the past of the left and right hemisphere signals from both BA 7 and 18. Cognitively relevant frequency bands included theta (4–7Hz), alpha (8–14Hz), beta (15–25Hz), and gamma (>25Hz) bands. We identified peaks within these bands for each individual, based on their cGC within the band (individual peak, IP). Theta was chosen as IP ± 2 for IP within 4–7.9 Hz, alpha IP ± 2 for IP within 8–14.9 Hz, beta IP ± 5 for IP within 15–24.9 Hz, and gamma IP ± 5 for IP within 25–50 Hz. Note that the same model was used for both time and frequency domain analyses. The results were qualitatively the same whether individually defined bands or the full, traditionally defined bandwidths were used.

**Statistical analysis—**A parametric analysis of variance (ANOVA) with Task (2 levels, Location task and TD task) and Trial type (*Load 2* and *Load 4* for Location task and *Load 2* and *Load 2D* for TD task; levels nested in Task) as factors and subjects as observations was used to analyze the behavioral performance (the dependent variable). An omnibus ANOVA with Greenhouse-Geisser correction was used to analyze the time-domain cGC data. Here, within-subjects factors were Task (Location task and TD task), Trial type (*Load 2* and *Load 4* for Location task and *Load 2* and *Load 2D* for TD task; levels nested in Task), and

Connections (6 levels, shown in Fig. 2C). Subjects were used as observations. Post hoc comparisons were used to interpret the factors driving any significant interactions found. All pairwise comparisons were made using Wilcoxon Signed Rank tests. Approximated *z* values are reported along with *p* values. Cohen's *d* is reported for parametric statistics and effect size (*r*) is reported for signed rank tests.

To compare cGC-based effective connectivity within-task conditions, we planned to test the differences in time domain-derived cGC between *Load 4* and *Load 2* and between *Load 2d* and *Load 2* for all six connections in the model ($H$=6; Fig. 2C). Because these planned comparisons represent just a few out of many possible comparisons, after reporting the results with correction for multiple comparisons, we also report the results of these a priori defined comparisons without correction for multiple comparisons. Note that six tests were done for each task. *Z* values are reported along with uncorrected *p* values. Furthermore, if significant trial-type related differences in the time-domain cGC at particular connections were found, we planned to follow up with post hoc analyses in the frequency domain, to assess whether different patterns of connectivity may be preferentially implemented via discrete frequency channels (Bastos et al., 2012). To do this, we compared the difference in frequency-domain cGC between trial types within each task for each frequency band (4 bands) only for significant connections found in the time-domain analysis.

## RESULTS

### Behavioral analysis

A complete set of behavioral data was acquired from 26 participants. Performance on *Load 2* trials was better than on *Load 4* trials (Table 1; $p<0.001$) for the location VSTM task. In the TD task, there was a main effect of Load (Table 1; $p<0.001$) such that performance on *Load 2d* trials was better than on *Load 4* trials ($t(18)=-5.05$, $p<0.001$), but performance on *Load 2d* trials was worse than the *Load 2* ($t(18)=4.53$, $p<0.001$).

### Connectivity analysis

Electrophysiological data was acquired from 19 subjects for the Location task and 18 subjects for the TD task. Analysis of network dynamics indicated that, overall, performance of both of the tasks produced robust patterns of bidirectional Granger causal interactions between each of the nodes in the network. Evidence that these patterns differed across tasks was revealed in the omnibus ANOVA. This analysis showed a main effect of Task ($F_{1,17}=5.71$, $p=0.03$), no main effect of Trial(Task) ($F_{2,34}=3.12$, $p=0.06$), a main effect of Connection ($F_{5,85}=5.84$, $p=.0001$), a significant Task*Connections interaction ($F_{5,255}=2.73$, $p=0.02$), and no significant Trial(Task)*Connection interaction ($F_{10,255}=0.43$, $p=0.93$). Visual inspection, followed up by pairwise comparisons, suggested that the connection from BA18 to BA9 ($z=-2.90$, uncorrected $p=0.003$, corrected $p=0.018$, $r=0.67$) was driving the interaction between Task and Connections such that the bottom-up connection was stronger for the task emphasizing load as compared to the task emphasizing the effects of distraction (Fig. 3). From here we conducted pairwise comparisons between the trial types for connections within each Task. All cGC measures are first reported for the data in the time domain, then with follow-up analyses in the frequency domain.

### Location VSTM task

Planned analyses ($N$=19 subjects) showed that cGC from BA 9 to 7 was stronger for *Load 4* versus *Load 2* ($z$=−2.52, uncorrected $p$=0.01, corrected $p$=0.06, $r$=0.58; Fig. 4 A and B). Following up on the time-domain finding, analyses in the frequency domain indicated that the load effect in the time domain was mirrored in the alpha band-specific cGC from BA 9 to 7, for which the cGC for *Load 4* was greater than for *Load 2* ($z$=−2.05, uncorrected $p$=0.04, corrected $p$=0.96, $r$=0.47, Fig. 4 C and D). There was no significant correlation between change in accuracy (*Load 4 – Load 2*) and the change in alpha band-specific cGC from BA 9 to BA 7 (*Load 4 – Load 2*). This was also true for the correlation using RT data.

### TD task

Planned analyses ($N$=18 subjects, one subject excluded because cGC values were > 3 *SD* above the mean) showed that cGC was larger for *Load 2d* versus *Load 2* for both the BA 9 to 18 connection ($z$=2.23, uncorrected $p$=0.02, corrected $p$=0.12, $r$=0.53; Fig. 5 A and B) and the BA 7 to 18 connection ($z$=2.24, uncorrected $p$=0.02, corrected $p$=0.12, $r$=0.53; Fig. 5 A and B). These effects were mirrored in the beta band-specific cGC from BA 9 to 18 (*Load 2d>Load 2*, $z$=2.24, uncorrected $p$=0.02, corrected $p$=0.48, $r$=0.53) and from BA 7 to 18 (*Load 2d>Load 2*, $z$=2.37, uncorrected $p$=0.02, corrected $p$=0.48, $r$=0.53; Fig. 5 D, E and F).

Additionally, cGC from BA 7 to 9 was larger for *Load 2d* versus *Load 2* in the time domain ($z$=2.26, uncorrected $p$=0.008, corrected $p$=0.048, $r$=0.53; Fig. 5 A and B). These effects were mirrored post hoc in both the alpha band-specific cGC from BA 7 to 9 (*Load 2d > Load 2*, $z$=2.54, uncorrected $p$=0.01, corrected $p$=0.24, $r$=0.60, Fig. 5 C and F and theta band-specific cGC from BA 7 to 9 (*Load 2d > Load 2*, $z$=2.50, uncorrected $p$=0.01, corrected $p$=0.24, $r$=0.59, Fig. 5 C and F).

There was no significant correlation between change in accuracy (*Load 2d – Load 2*) and the change in beta band-specific cGC from BA 7 to 18 (*Load 2d – Load 2*). This was also true for the beta band-specific cGC from BA 9 to 18, the theta band-specific cGC from BA 7 to 9, and the alpha band-specific cGC from BA 7 to 9. Analogous correlation between RT and cGC for the connections listed above were not significant.

## DISCUSSION

Behavioral evidence suggests that there exist dissociable processes underlying VSTM that relate to processes underlying visual selective attention (Machizawa and Driver, 2011). Here, we tested the hypothesis that two of these behaviorally dissociable constructs of VSTM -- capacity and filtering-- are supported by different network dynamics within the frontoparietal system, and between these regions and extrastriate occipital cortex. To address this question, we measured the casual connectivity patterns present within a set of network connections that are engaged during the delay-period of two STM tasks operationalizing these two cognitive constructs. Our results support the broad prediction that the mechanisms underlying capacity and filtering are implemented, in part, via different dynamically configured functional networks supported by a common anatomical substrate.

At the level of task, collapsing across within-task manipulations, the load task engaged stronger bottom up connectivity (specifically, from BA 18 to BA 9) compared to the distraction filtering task (Fig. 3). Our findings within the load task suggest that VSTM capacity (which may be isomorphic with alerting in attention) is supported by a pattern of increased drive from dlPFC on SPL during maintenance of larger mnemonic loads (Fig. 4). This finding adds a layer of specificity to our previous finding, with TMS-EEG, that these regions exhibit strengthened casual connectivity during *Load 4* vs. *Load 2* trials. The present results also suggest that this dlPFC-to-SPL influence may be carried preferentially in the alpha frequency band. A different pattern was observed for filtering (which may be isomorphic with executive control of attention), as operationalized in the distraction task. For each significant connection in the network there was greater connectivity for trials with distraction compared to trials with equivalent mnemonic load, but no distraction. The results broke out into anterior-to-posterior and posterior-to-anterior connections (Fig. 5). Greater top-down influence was seen from dlPFC to extrastriate cortex and from SPL to extrastriate cortex, in both cases with a prominent component in the beta frequency band. Additionally, distraction was associated with greater influence of SPL on dlPFC, an effect that was prominent in the theta and alpha frequency bands. Univariate analyses did not reveal significant associations between measures of behavioral performance and measures of connectivity for either task, though it is possible that multivariate approaches maybe be more revealing. Such analyses are beyond the score of this study. One caveat of this work is that no conclusions can be drawn regarding any possible hemispheric specificity of these results.

Our findings are consistent with a considerable body evidence that prefrontal and parietal areas regulate earlier visual areas during VSTM and visual selective attention (Gazzaley and Nobre, 2012), including causal demonstrations effected by altering prefrontal or parietal activity using low frequency (1 Hz; Zanto et al., 2011) or theta burst (Lee and D'Esposito, 2012) repetitive TMS. Furthermore, cortical cooling methods have been used to demonstrate reciprocal regulation between parietal and prefrontal areas during performance of an oculomotor delayed-response task (Chafee and Goldman-Rakic, 2000). However, these functional lesion studies do not provide information about patterns of directed causal influence between brain areas, in part a consequence of the fact that most neural systems feature a large number of feedback loops and compensatory mechanisms that help maintain stable function. A demonstration of this fact is seen in Lee et al. (2012), in which theta burst rTMS applied to one hemisphere of dlPFC during an STM task disrupted performance, but the preserved performance was associated with increased activity in the homologous region of the contralateral hemisphere (Lee and D'Esposito, 2012). For insight about the dynamics of interareal regulation, one must turn to data from functional studies. A model that is emerging from electrophysiological investigations is that top-down control may be implemented through different "frequency channels" that, much like a radio, can selectively modulate the frequency band engaged, depending on the cognitive context (Palva et al., 2011; Miller and Buschman, 2013). The present results are consistent with this model, and offer a greater level of specificity for the case of VSTM. Additionally, our results provide a link between the functional-lesion and electrophysiology literatures, suggesting that

interareal control may be accomplished via context-specific, dynamically configured patterns of connectivity.

Distractors presented during the encoding period created a perceptually identical, but cognitively different, delay-period compared to the location VSTM task. In this context, we found engagement of the same brain areas, but via a different network configuration compared to that of the capacity condition (Fig. 5). This observation invites a comparison with findings using the contralateral delay activity (CDA), an event-related potential derived from the EEG that indexes individual differences in VSTM capacity (Vogel and Machizawa, 2004). The CDA has also been shown to vary with distraction presented during encoding, in the following way: for low capacity subjects, the CDA associated with the *Load 2d* condition is similar to that of the *Load 4* condition, whereas, for high VSTM capacity subjects, the CDA for *Load 2d* is the same as that of the *Load 2* condition (Vogel et al., 2005). The authors suggest that VSTM capacity limitations may depend on filtering efficiency, and not just on how much "space" is available for VSTM maintenance. Although it is possible that there is a common mechanism by which information is selected for encoding such that a bottleneck affects both filtering efficiency and VSTM capacity, the uni-dimensional nature of the CDA prevents it from being able to discern whether one or multiple mechanisms contribute to the theoretically dissociable constructs of capacity and filtering. By employing our measures of network connectivity, in contrast, we have been able to demonstrate that a broadly distributed anatomical network takes on distinct dynamic configurations during tasks that emphasize capacity versus filtering.

Interestingly, the top-down filtering effects that we observed were prominent in the beta frequency band. The beta-band has been implicated in top-down control of attention and aspects of STM (Engel and Fries, 2010; Miller and Buschman, 2013, Bressler and Richter, 2014). Higher beta-band coherence is found between dlPFC and parietal areas during conjunction search using selective attention, a cognitively top-down process, versus pop-out search, a cognitively bottom-up process (Buschman and Miller, 2007). Our results are also in line with the findings of Zanto et al. (2009) who reported increased beta-band desynchronization during the delay-period in parietal areas that was related to the inability to filter out distraction.

In summary, our results suggest that a common anatomical substrate – dlPFC, parietal cortex, and extrastriate occipital cortex – may support different control operations in a context-dependent manner by dynamic reconfiguration of patterns of frequency-specific connectivity.

## ACKNOWLEDGEMENTS

This research was conducted using the High-Throughput Computing Center at the University of Wisconsin-Madison. All work was conducted at University of Wisconsin-Madison and was supported by MH095428 (B.K.), MH095984 (B.R.P), MH064498 (B.R.P.) from the National Institutes of Health, and EB009749 (B.D.V.) and EB015542 (B.D.V.) from the National Institute of Biomedical Imaging and Bioengineering.

## Abbreviations

| | |
|---|---|
| **STM** | Short-term memory |
| **EEG** | electroencephalogram |
| **VSTM** | visual short-term memory |
| **ERP** | event-related potential |
| **CDA** | contralateral delay activity |
| **CSA** | contralateral search activity |
| **TMS** | transcranial magnetic stimulation |
| **dlPFC** | dorsolateral prefrontal cortex |
| **SPL** | superior parietal lobule |
| **cGC** | conditional Granger causality |
| **TD** | target-epoch distraction |
| **ITI** | intertrial interval |
| **BEM** | boundary-element model |
| **EM** | expectation-maximization |
| **MVAR** | multivariate autoregressive |
| **ICA** | independent components analysis |

## REFERENCES


Bastos AM, Usrey WM, Adams RA, Mangun GR, Fries P, Friston KJ. Canonical microcircuits for predictive coding. Neuron. 2012; 76(4):695–711. [PubMed: 23177956]

Bressler SL, Seth AK. Wiener-Branger Causality: A well established methodology. NeuroImage. 2011; 58(2):323–329. [PubMed: 20202481]

Bressler SL, Richter CG. Interareal oscillatory synchronization in top-down neocortical processing. Curr Opin Neurobiol. 2015; 31:62–66. [PubMed: 25217807]

Buschman TJ, Miller EK. Top-down versus bottom-up control of attention in the prefrontal and posterior parietal cortices. Science. 2007; 315:1860–1862. [PubMed: 17395832]

Casali AG, Casarotto S, Rosanova M, Mariotti M, Massimini M. General indices to characterize the electrical response of the cerebral cortex to TMS. Neuroimage. 2010; 49:1459–1468. [PubMed: 19770048]

Chafee MV, Goldman-rakic PS. Inactivation of Parietal and Prefrontal Cortex Reveals Interdependence of Neural Activity During Memory-Guided Saccades. J Neurophysiol. 2000; 83:1550–1566. [PubMed: 10712479]

Chen Y, Bressler SL, Ding M. Frequency decomposition of conditional Granger causality and application to multivariate neural field potential data. J Neurosci Methods. 2006; 150:228–237. [PubMed: 16099512]

Cheung BLP, Riedner BA, Tononi G, Van Veen BD. Estimation of cortical connectivity from EEG using state-space models. IEEE Trans Biomed Eng. 2010; 57:2122–2134. [PubMed: 20501341]

Cowan N, Elliott EM, Scott Saults J, Morey CC, Mattox S, Hismjatullina A, Conway ARa. On the capacity of attention: its estimation and its role in working memory and cognitive aptitudes. Cogn Psychol. 2005; 51:42–100. [PubMed: 16039935]

Cusack R, Lehmann M, Veldsman M, Mitchell DJ. Encoding strategy and not visual working memory capacity correlates with intelligence. Psychon Bull Rev. 2009; 16:641–647. [PubMed: 19648446]

Dentico D, Cheung BL, Chang JY, Guokas J, Boly M, Tononi G, Van Veen BD. Reversal of cortical infomraiton flow during visual imagery as compared to visual perception. NeuroImage. 2014; 100:237–243. [PubMed: 24910071]

Emrich SM, Al-Aidroos N, Pratt J, Ferber S. Finding memory in search: the effect of visual working memory load on visual search. Q J Exp Psychol. 2010; 63:1457–1466. (2006).

Engel AK, Fries P. Beta-band oscillations--signalling the status quo? Curr Opin Neurobiol. 2010; 20:156–165. [PubMed: 20359884]

Fan J, McCandliss BD, Sommer T, Raz A, Posner MI. Testing the efficiency and independence of attentional networks. J Cogn Neurosci. 2002; 14:340–347. [PubMed: 11970796]

Friston KJ. Functional and Effective Connectivity in Neuroimaging: A synthesis. Hum Brain Mapp. 1994; 2:56–78.

Friston KJ. Functional and Effective Connectivity: A Review. Brain Conn. 2011; 1(1):13, 36.

D'Esposito M, Postle BR. The Cognitive Neuroscience of Working Memory. Annu Rev Psychol. 2015; 66:28.1–28.28.

Gazzaley A, Nobre AC. Top-down modulation: bridging selective attention and working memory. Trend Cogn Sci. 2012; 16:129–135.

Geweke JF. Measures of Conditional Linear Dependence and Feedback Between Time Series. J Am Statistical Assoc. 1984; 79:907–915.

Ikkai A, Curtis CE. Common neural mechanisms supporting spatial working memory, attention and motor intention. Neuropsychologia. 2011; 49:1428–1434. [PubMed: 21182852]

Jerde, Ta; Merriam, EP.; Riggall, AC.; Hedges, JH.; Curtis, CE. Prioritized maps of space in human frontoparietal cortex. J Neurosci. 2012; 32:17382–17390. [PubMed: 23197729]

Kundu B, Sutterer DW, Emrich SM, Postle BR. Strengthened effective connectivity underlies transfer of working memory training to tests of short-term memory and attention. J Neurosci. 2013; 33:8705–8715. [PubMed: 23678114]

Lee TG, D'Esposito M. The dynamic nature of top-down signals originating from prefrontal cortex: a combined fMRI-TMS study. J Neurosci. 2012; 32:15458–15466. [PubMed: 23115183]

Limpiti T, Van Veen BD, Wakai RT. Cortical patch basis model for spatially extended neural activity. IEEE Trans Biomed Eng. 2006; 53:1740–1754. [PubMed: 16941830]

Machizawa MG, Driver J. Principal component analysis of behavioural individual differences suggests that particular aspects of visual working memory may relate to specific aspects of attention. Neuropsychologia. 2011; 49:1518–1526. [PubMed: 21130786]

Malekpour S, Li Z, Cheung BLP, Castillo EM, Papanicoulaou AC, Kramer LA, Fletcher JM, Van Veen BD. Interhemispheric Effective and Functional Cortical Connectivity Signatures of Spina Bifida Are Consistent with Callosal Anomaly. Brain Conn. 2012; 2:142–155.

Miller BT, D'Esposito M. Searching for "the top" in top-down control. Neuron. 2005; 48:535–538. [PubMed: 16301170]

Miller EK, Buschman TJ. Cortical circuits for the control of attention. Curr Opin Neurobiol. 2013; 23:216–222. [PubMed: 23265963]

Nobre AC, Stokes MG. Attention and short-term memory: crossroads. Neuropsychologia. 2011; 49:1391–1392. [PubMed: 21571124]

Palva JM, Monto S, Kulashekhar S, Palva S. Neuronal synchrony reveals working memory networks and predicts individual memory capacity. Proc Natl Acad Sci U S A. 2010; 107:7580–7585. [PubMed: 20368447]

Piantoni G, Cheung BLP, Van Veen BD, Romeijn N, Riedner BA, Tononi G, Van Der Werf YD, Van Someren EJW. Disrupted directed connectivity along the cingulate cortex determines vigilance after sleep deprivation. Neuroimage. 2013; 79C:213–222. [PubMed: 23643925]

Postle BR. Working memory as an emergent property of the mind and brain. Neuroscience. 2006; 139:23–38. [PubMed: 16324795]

Uhlhaas PJ, Pipa G, Lima B, Melloni L, Neuenschwander S, Nikolic D, Lin S. Neural synchrony in cortical networks : history , concept and current status. Front Integr Neurosci. 2009; 3:1–19. [PubMed: 19225578]

Vogel EK, Machizawa MG. Neural activity predicts individual differences in visual working memory capacity. Nature. 2004; 428:748–751. [PubMed: 15085132]

Vogel EK, McCollough AW, Machizawa MG. Neural measures reveal individual differences in controlling access to working memory. Nature. 2005; 438:500–503. [PubMed: 16306992]

Zanto TP, Gazzaley A. Neural suppression of irrelevant information underlies optimal working memory performance. J Neurosci. 2009; 29(10):3059–3066. [PubMed: 19279242]

Zanto TP, Rubens MT, Thangavel A, Gazzaley A. Causal role of the prefrontal cortex in top-down modulation of visual processing and working memory. Nat Neurosci. 2011; 14:656–661. [PubMed: 21441920]

## Highlights

- Granger causality-based connectivity measured between brain regions using EEG data
- STM maintenance and distraction filtering use different brain networks
- Maintenance uses dlPFC to SPL connection via the alpha band
- Filtering uses dlPFC to extrastriate and SPL to extrastriate connections via beta
- Filtering also uses the SPL to dlPFC connection via the alpha and theta bands

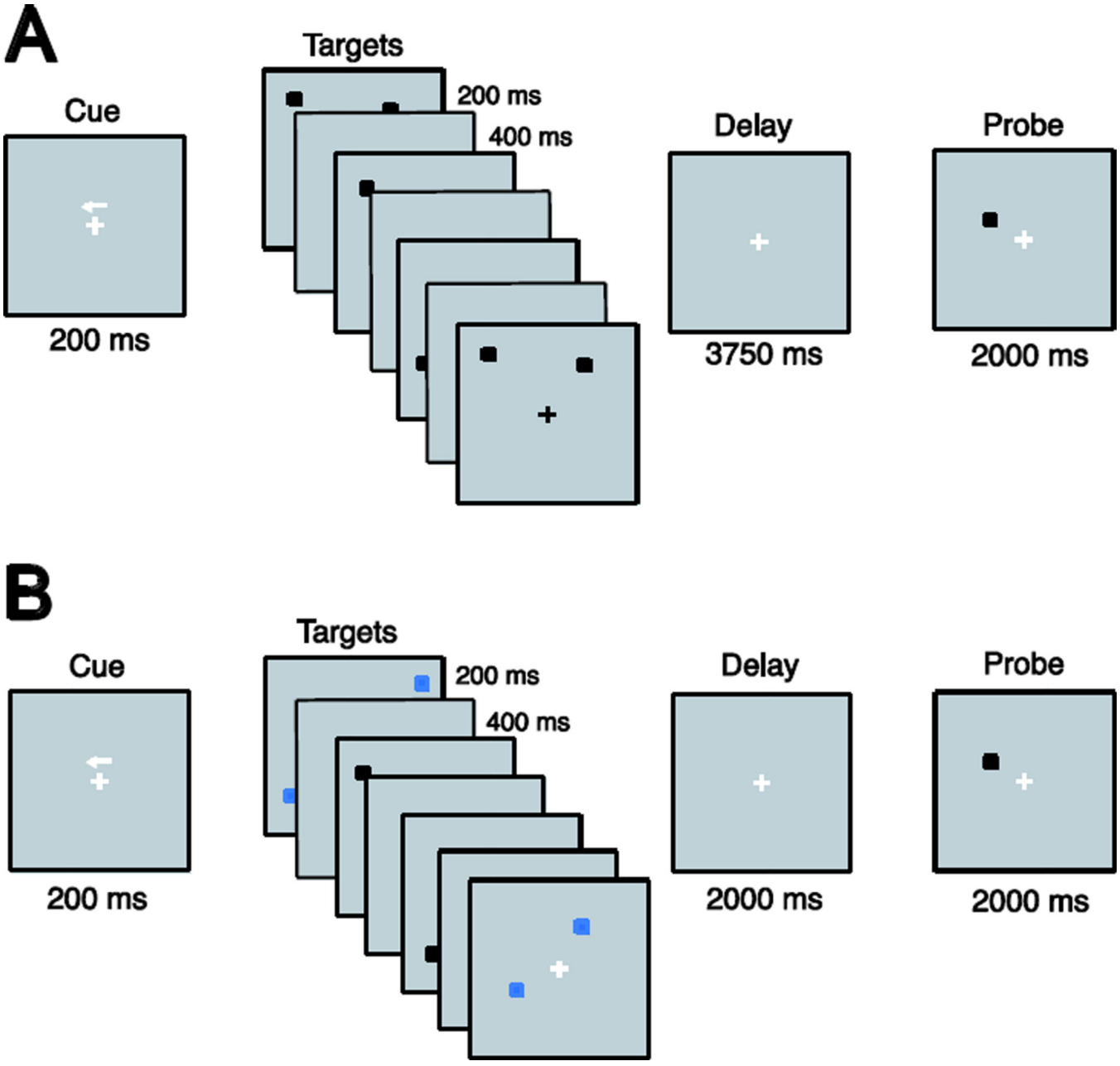


**Figure 1. Schematic representation of tasks**

(**A**) Location VSTM task. Example of a *Load 4* trial. Memory targets ("targets" in the figure) were black, as was the probe. (**B**) Target-distraction (TD) task. Example of a *Load 2d* trial. In this task relevant stimuli were presented in black and irrelevant stimuli in blue.

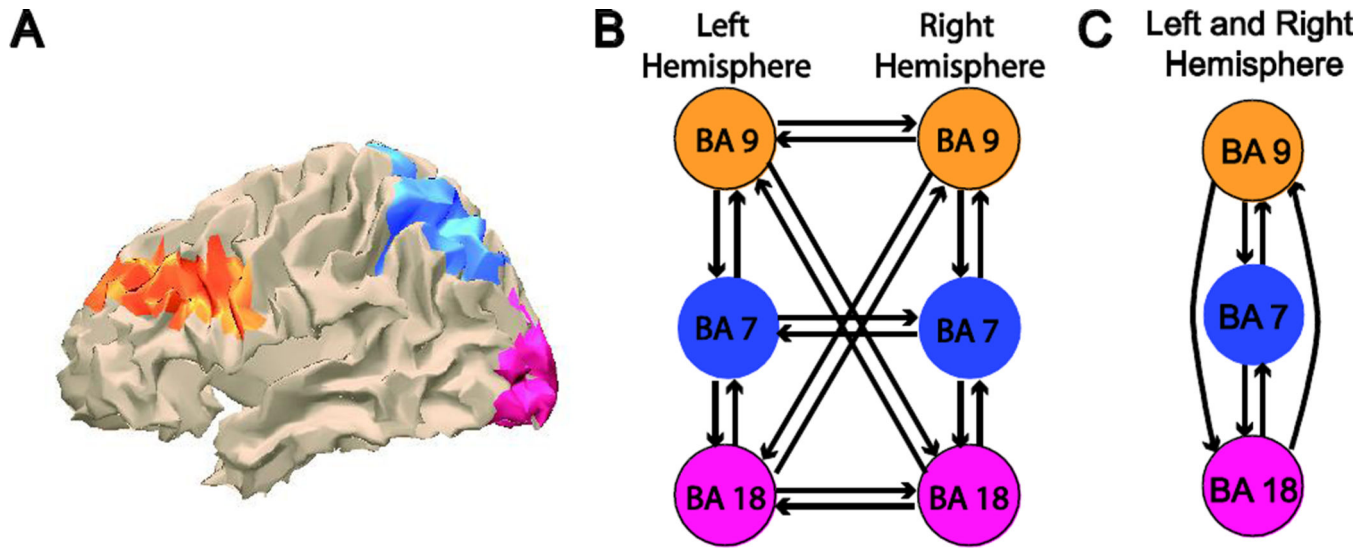


**Figure 2. MVAR model**

**(A)** Brain regions included in the model labeled on an MNI template brain. (**B**) Full model connections. Black arrows indicate connections tested. Colors follow from panel A. (**C**) Simplified model that is collapsed over hemispheres.

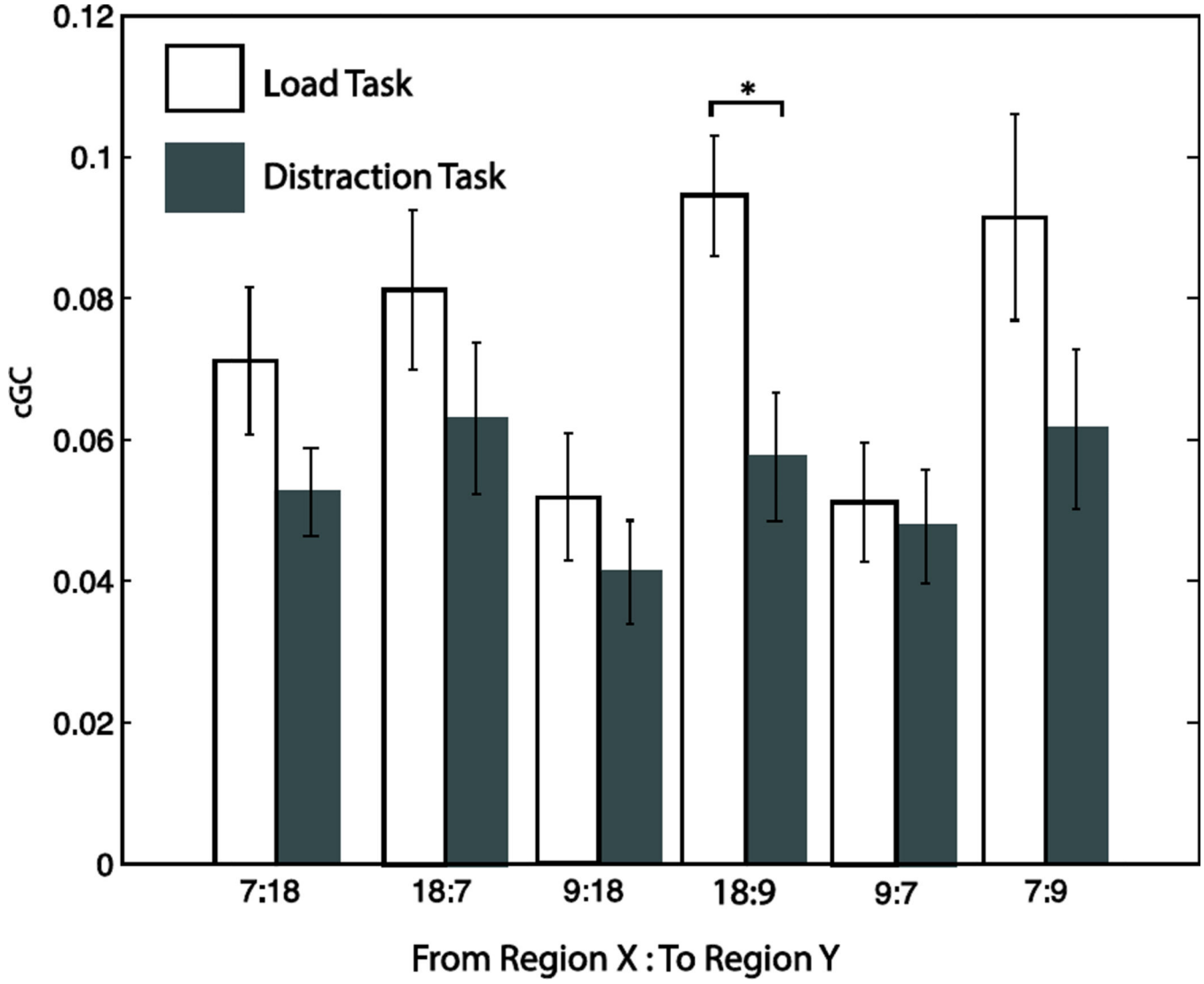


**Figure 3. cGC for Location task versus Distraction task, Task x Connection interaction**

cGC during the delay-period in the time domain for the Location task, bar represents mean cCG collapsed over trial type (*Load 2* and *Load 4;* white) and the TD task, bar represents mean cCG collapsed over trial type (*Load 2* and *Load 2d;* gray).

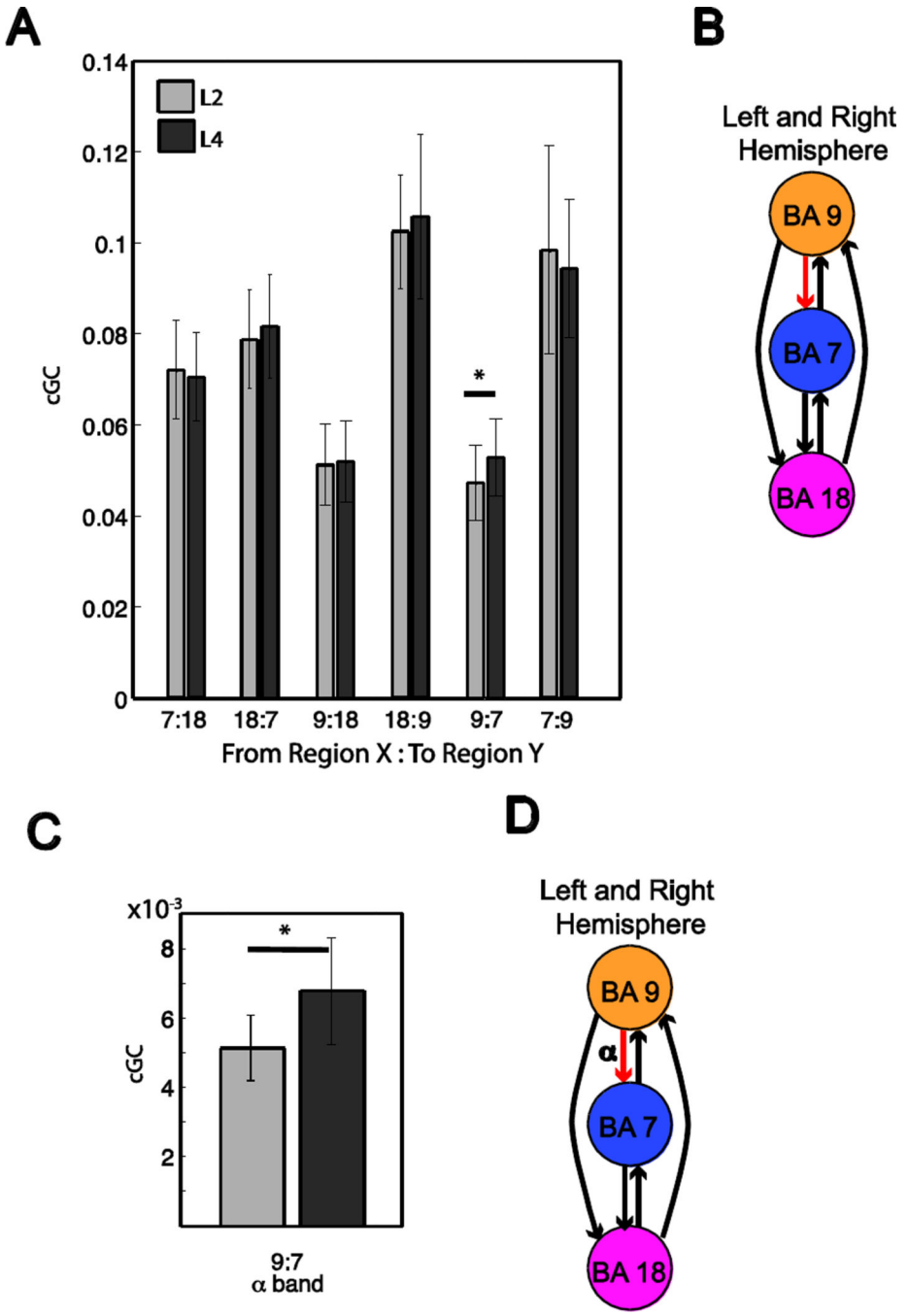


**Figure 4. cGC from the location VSTM task**

(**A**) cGC during the delay-period in the time domain, plotted for all connections and task conditions. (**B**) Schematic of significant connections present during delay-period for time domain-derived cGC, *Load 4>Load 2* (**C**) cGC in alpha frequency band during delay-period. (**D**) Schematic of significant connections present during delay-period of task for frequency domain-derived cGC. Same conventions for arrows as in panel B.

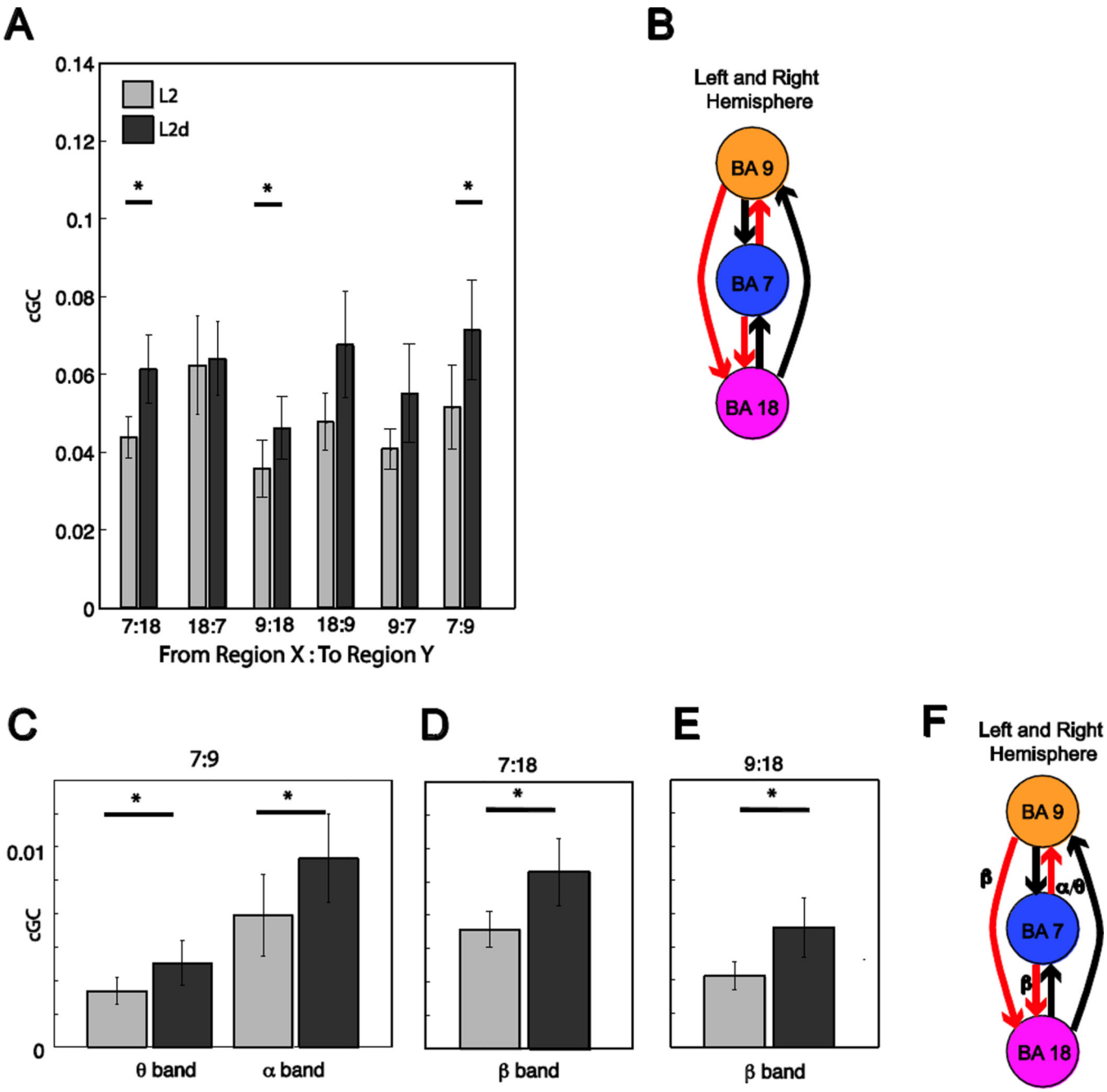


**Figure 5. cGC from the TD VSTM task**

**(A)** cGC in the time domain, plotted for all connections and task conditions. **(B)** Schematic of significant connections present during delay-period of task for the time domain-derived cGC. Red arrows indicate connections that show a significant difference between distraction and no distraction conditions, *Load 2d>Load 2*. **(C–E)** cGC of the designated frequency band plotted for connections that showed significant difference between trial types. **(F)** Schematic of significant connections present during the delay-period of the task for the frequency domain-derived cGC. Same arrow conventions as in panel B.

**Table 1**

Performance on tasks.

| Task | Condition | Mean (SD) | F value (df,df) | Cohen's d (95% CI) | p value |
|---|---|---|---|---|---|
| **Location VSTM task** | | | | | |
| ACC | *Load 2* | 0.79 (0.07) | 26.48 (1,36) | 2.36 (1.12, 3.53) | <0.001 |
| | *Load 4* | 0.67 (0.07) | | | |
| RT | *Load 2* | 795.16 (157) | 0.65 (1,36) | 0.37 (−0.5, 1.27) | 0.42 |
| | *Load 4* | 835.80 (153) | | | |
| **TD task** | | | | | |
| ACC | *Load 2* | 0.82 (0.07) | 20.29 (2,75) | 2.06 (1.25, 2.87) | <0.001 |
| | *Load 4* | 0.68 (0.07) | | | |
| | *Load 2d* | 0.78 (0.07) | | | |
| RT | *Load 2* | 780.52 (118) | 1.28 (2,75) | −0.37 (−1.0, 0.29) | 0.28 |
| | *Load 4* | 818.54 (122) | | | |
| | *Load 2d* | 765.84 (114) | | | |

ACC: Accuracy
RT: Reaction Time